A&A 421, 1075–1086 (2004)
DOI: 10.1051/0004-6361:20040284

Astronomy & Astrophysics

The effect of dust settling on the appearance of protoplanetary disks

C. P. Dullemond[1] and C. Dominik[2]

[1] Max Planck Institut für Astrophysik, PO Box 1317, 85741 Garching, Germany
[2] Sterrenkundig Instituut "Anton Pannekoek", Kruislaan 403, 1098 SJ Amsterdam, The Netherlands
e-mail: dominik@science.uva.nl

Received 17 February 2004 / Accepted 1 April 2004

Abstract. We analyze how the process of dust settling affects the spectral energy distribution and optical appearance of protoplanetary disks. Using simple analytic estimates on the one hand, and detailed 1+1-D models on the other hand, we show that, while the time scale for settling down to the equator may exceed the life time of the disk, it takes much less time for even small grains of 0.1 μm to settle down to a few pressure scale heights. This is often well below the original location of the disk's photosphere, and the disk therefore becomes effectively "flatter". If turbulent stirring is included, a steady state solution can be found, which is typically reached after a few $\times 10^5$ years. In this state, the downward settling motion of the dust is balanced by vertical stirring. Dependent on the strength of the turbulence, the shape of the disk in such a steady state can be either fully flaring, or flaring only up to a certain radius and self-shadowed beyond that radius. These geometries are similar to the geometries that were found for disks around Herbig Ae/Be stars in our previous papers (Dullemond 2002, A&A, 395, 853; Dullemond & Dominik 2004, A&A, 417, 159, henceforth DD04). In those papers, however, the reason for a disk to turn self-shadowed was by loss of optical depth through dust grain growth. Here we show that dust settling can achieve a similar effect without loss of vertical optical depth, although the self-shadowing in this case only affects the outer regions of the disk, while in DD04 the entire disk outside of the puffed-up inner rim was shadowed. In reality it is likely that both grain growth and grain settling act simultaneously. The spectral energy distributions of such self-shadowed – or partly self-shadowed – disks have a relatively weak far-infrared excess (in comparison to flaring disks). We show here that, when dust settling is the cause of self-shadowing, these self-shadowed regions of the disk are also very weak in resolved images of scattered light. A reduction in the brightness was already predicted in DD04, but we find that dust settling is far more efficient than grain growth at dimming the scattered light image of the disk. Settling is also efficient in steepening the spectral energy distribution at mid- to far-infrared wavelengths. From the calculations with compact grains it follows that, after about 10^6 years, most disks should be self-shadowed. The fact that some older disks are still observed with the characteristics of flaring disks therefore seems somewhat inconsistent with the time scales predicted by the settling model based on compact grains. This suggests that perhaps even the small grains ($\lesssim 0.1$ μm) have a porous or fractal structure, slowing down the settling. Alternatively, it could mean that the different geometries of observed disks is merely a reflection of the turbulent state of these disks.

Key words. accretion, accretion disks – ISM: dust, extinction – turbulence

1. Introduction

The dusty circumstellar disks surrounding most T Tauri stars and Herbig Ae/Be stars are believed to be the birthplace of planetary systems. These systems are therefore the object of intense study, both observationally and theoretically. Much of what we know of these systems has been derived indirectly from their spectral energy distributions and infrared spectra. In the last few years the amount of observational information on spatial structure of these objects has increased dramatically. The outer disk regions (typically outside of 50 AU) can be probed by direct imaging, both at optical/near-infrared wavelengths with HST/STIS (e.g., Augereau et al. 2001; Grady et al. 1999), and in the sub-mm regime (Mannings & Sargent 1997), and with near- and mid-infrared interferometry the inner disk structures can be probed (e.g., Eisner et al. 2003; Millan-Gabet et al. 2001; Leinert et al. 2004).

Models of protoplanetary disks are increasingly successful at accounting for much of the observed properties. For instance, they can explain why their spectral energy distributions (SEDs) are generally rather flat in νF_ν (Kenyon & Hartmann 1987), why dust features are almost always observed in emission (Calvet et al. 1991; Chiang & Goldreich 1997), what the meaning is of the near-infrared bump in the SEDs of Herbig Ae stars (Natta et al. 2001; Dullemond et al. 2001), and why some sources have strong and some have weak far-IR

Send offprint requests to: C. P. Dullemond,
e-mail: dullemon@mpia-hd.mpg.de

excess (Dullemond 2002; Dullemond & Dominik 2004, henceforth DD04).

For the overall disk properties, it is often sufficient to work with a disk model in which dust and gas are well mixed and coupled. However, there are indications that dust growth, thermal processing, and dust-gas separation can play an important role in disks. The different overall shapes of the SEDs of Herbig AeBe stars (the "group I" and "group II" spectra identified by Meeus et al. 2001) can be understood by a reduction in opacity in the outer disk via grain growth (DD04; see also D'Alessio et al. 2001) or a direct reduction of the disk height by settling of small grains (Chiang et al. 2001). The high submm fluxes observed in disks with relatively low far-IR fluxes can be explained by a component of large grains in the disk interior which do not contribute to the opacity high above the midplane but contribute only as a cold component to the submm emission (Natta et al. 2001; DD04). Both grain growth and grain settling is required to understand the presence of these grains. Moreover, the infrared spectra taken from the ground and from space have revealed structure in the infrared dust emission features that are indicative of dust grain growth and thermal processing (Bouwman 2001; van Boekel 2003; Honda et al. 2003; Meeus et al. 2003; Przygodda et al. 2003).

Also from a theoretical point of view, grain processing and dust-grain separation are expected to occur. In fact, a central role in our current understanding of planet formation is played by the formation of a *dust subdisk* within the disk (28; 9). Dust grains tend to settle towards the midplane, unless this process is countered by strong vertical stirring in the disk. The formation of such a subdisk with enhanced dust density greatly influences the timescales in which dust grains may grow to planetesimals and eventually planets. For the detailed structure of the dust subdisk, parameters like the remaining accretion rate, local turbulence, radial mixing processes, etc. play and important role (9; 7). Unfortunately, the processes that generate turbulence in protoplanetary disks are not well understood, and mixing/stirring is generally treated in a simple parameterized manner.

One way to approach this problem is to search for observational signs of dust settling in disks. Observations of disks, at least in the optical and infrared, mostly probe the upper disk layers. If settling is active in disks, the upper layers of a disk will be influenced and may show observable changes. While there are many studies into the effects of settling onto the dust distribution relevant for planet formation (see e.g., Takeuchi & Lin 2002, 2003), there are curiously few studies which discuss the observational consequences of dust settling in a quantitative way. A study of this kind was presented by Miyake & Nakagawa (1995, hereafter MN95). They studied the effects of grain settling and accretion luminosity on the SED of T Tauri disks in order to explain the infrared and IRAS colors of these stars. However, their study is limited in several ways. MN95 did not consider turbulent stirring at all. The basic assumption of their model was that turbulence has completely ceased and dust settling can proceed undisturbed. The dust was assumed to be confined within one pressure scale height, and the time scales for changing the surface height in the disk were computed using the midplane density. These time scales turn out to be between 10^5 and 10^7 years, and therefore comparable to the lifetime of protoplanetary disks. However, the timescales for settling are much shorter in the higher layers of the disk. Moreover, we will show that turbulence prevents the dust from settling down below a certain height, often much larger than the pressure scale height, and that turbulence will therefore determine the final shape of the photospheric surface of the disk.

In this paper we investigate the effects of dust settling in the presence of turbulent stirring on the observable quantities of protoplanetary disks, in particular their SEDs and their images in scattered light. To do this we start with a well-mixed disk model for a T Tauri star and compute how the process of dust settling proceeds. In all stages of this process we compute observable quantities and see how they change. In doing this we hope to find typical observable signatures of dust settling which can be used to analyze protoplanetary disks.

The paper is organized as follows: in Sect. 2 we use simple analytical estimates to derive the timescales for settling and stirring. In Sect. 3 we solve the equations for settling and stirring in a one-dimensional slab, a vertical cut through the disk and show how quickly the upper layers of the disk are depleted and to what depth. In Sect. 4 we run a similar calculation at all locations in the disk and compute the changes settling causes to both the SED and images in scattered light.

2. Settling, vertical stirring and accretion

The equations for settling, vertical stirring and accretion have been extensively discussed in the literature. But, for the sake of clarity, and to define our notation, we include a brief discussion of the entire set of equations used for the current study.

Dust grains in a protoplanetary disk experiences a gravitational force towards the star. If it were not for the gas in the disk, the grains would move on inclined orbits. In a corotating frame this means they would oscillate about the midplane with the Keplerian frequency. However, small grains have a large surface-to-mass ratio, and therefore experience strong drag forces with the gas. Instead of oscillating about the midplane, these grains slowly settle toward the midplane on a time scale of a few hundred thousand years. This time scale depends on the surface density of the gas and on the surface-to-mass ratio of the grain. Large compact grains have a much smaller surface-to-mass ratio and therefore tend to settle on a much shorter time scale. Settling can, however, only take place when turbulence in the disk does not stir up the grains above the midplane again. Usually this happens up to a certain height $z_{\rm sett}$ above the midplane while above this height the settling can proceed without problems. This means that after a certain settling time, the disk above $z_{\rm sett}$ is more or less devoid of dust grains of this particular size, while below it the vertical stirring has more or less equalized the abundance of dust grains of this size.

In this section we derive the equations for these processes, and estimate the height $z_{\rm sett}$ and the time scale that it takes for the dust to settle down to this height.

2.1. Settling

The interaction between a dust grain and the surrounding gas can be described by the *friction time* which is the time scale in which a dust grain responds to the motion of the gas.

$$t_{\rm fric} = \frac{mv}{|F_{\rm fric}|} \tag{1}$$

where m is the mass of the dust particle and v the relative velocity between gas and dust. The friction force $F_{\rm fric}$ is a function of the drift velocity v, the grain properties and the gas density and temperature. In general, different regimes must be distinguished depending on the hydrodynamic regime appropriate for a given situation. However, for grains smaller than typically 1 cm, the Epstein regime is applicable throughout a protoplanetary disks (Cuzzi et al. 1993), so we restrict ourselves for the current paper to this regime. Then, under the generally valid assumption of subsonic drift velocities, the friction force is given by

$$F_{\rm fric} = -\frac{4}{3}\rho\sigma v c_{\rm s} \tag{2}$$

where ρ is the gas density, σ is the collisional cross section of the dust grain and $c_{\rm s}$ is the isothermal sound velocity

$$c_{\rm s} = \sqrt{\frac{kT_{\rm gas}}{\mu_{\rm gas}m_{\rm p}}}. \tag{3}$$

$T_{\rm gas}$ is the gas temperature, k the Boltzman constant, $\mu_{\rm gas}$ the mean molecular weight in the gas and $m_{\rm p}$ the proton mass. In the Epstein regime, the friction time can be written as

$$t_{\rm fric} = \frac{3}{4}\frac{m}{\sigma}\frac{1}{\rho c_{\rm s}}. \tag{4}$$

The friction time depends upon the dust grain properties through the mass-to-crosssection ratio m/σ. For compact spherical grains with grain radius a and specific density $\rho_{\rm d}$, $m/\sigma = 4\rho_{\rm d}a/3$, and the friction time turns into the familiar form $t_{\rm fric} = \rho_{\rm d}a/\rho c_{\rm s}$. However, through much of this paper we will continue to write m/σ since this expression is much more general and allows for a direct generalization towards 2-dimensional grains (like polycyclic aromatic hydrocarbons (PAHs)) and porous or fractal grains.

We now consider a circumstellar disk around a star with mass $M_\star$. We assume the disk to be isothermal in the vertical direction, and we make the thin-disk-approximation: $z \ll R$. At a distance R from the star, the vertical density distribution is then given by

$$\rho(z) = \frac{\Sigma}{\sqrt{2\pi}H_p}\exp\left(\frac{-z^2}{2H_p{}^2}\right) \tag{5}$$

where Σ is the surface density in the disk, H_p the pressure scale height and z the height above the disk. The pressure scale height is given by

$$H_p = \frac{c_{\rm s}}{\Omega_{\rm K}} \tag{6}$$

where $\Omega_{\rm K} = \sqrt{GM_\star/R^3}$ denotes the local Kepler frequency. A dust grain located at (R, z) is subject to a vertical gravitational force

$$F_{\rm grav} = -m\Omega_{\rm K}{}^2 z \tag{7}$$

and, in the absence of turbulent stirring, settles towards the midplane at a settling speed

$$v_{\rm sett} = -z\Omega_{\rm K}{}^2 t_{\rm fric} = -\frac{3\Omega_{\rm K}{}^2 z}{4\rho c_{\rm s}}\frac{m}{\sigma}, \tag{8}$$

which follows from $F_{\rm grav} = F_{\rm fric}$.

The settling speed decreases as one comes closer to the equator, because the gas density increases and the vertical component of the gravity decreases. The time for a grain to settle to a certain height z is therefore dominated by the local settling speed at height z

$$t_{\rm sett} = \frac{z}{v_{\rm sett}} = \frac{4}{3}\frac{\sigma}{m}\frac{\rho c_{\rm s}}{\Omega_{\rm K}{}^2}. \tag{9}$$

Using the vertical density distribution in Eq. (5), we find

$$t_{\rm sett} = \frac{4}{3\sqrt{2\pi}}\frac{\sigma}{m}\frac{\Sigma}{\Omega_{\rm K}}\exp\left(-\frac{z^2}{2H_p{}^2}\right). \tag{10}$$

The time for a grain to settle towards the midplane of a disk is therefore approximately given by $t_{\rm sett} = (4/3\sqrt{2\pi})(\sigma/m)(\Sigma/\Omega_{\rm K})$. However, it is important to know, that in the higher layers of the disk, the timescales are very different. Typical flaring disk models intercept stellar radiation at a height $z \sim 4H_p$. The local settling time scales in this region differ from the time scales close to the midplane by a factor $e^{-8} \approx 1/3000$. Therefore, dust settling will deplete the upper layers of a disk surface much faster than the actual formation time of the dust subdisk close to the midplane (see also Chiang & Goldreich 1997; Takeuchi & Lin 2002).

2.2. Vertical stirring

Vertical stirring occurs when the disk is turbulent. The turbulent eddies of the gas transport the dust grains up and down in a random manner, thus constituting a diffusion process for the dust. A detailed formulation of the theory behind this turbulent diffusion of dust grains is given by e.g. Völk et al. (1980); Weidenschilling (1997); Cuzzi et al. (1993); Dubrulle et al. (1995), and most recently by Schräpler & Henning (A&A submitted).

The diffusion coefficient for gas molecules D_0 is defined using the standard α prescription:

$$D_0 = \alpha c_{\rm s} H_p. \tag{11}$$

But dust particles may not always couple perfectly to the gas. The actual diffusion coefficient for dust particles of a certain size is:

$$D = \frac{D_0}{\rm Sc}, \tag{12}$$

where Sc is the Schmidt number. For perfectly coupled particles (i.e. infinitely small grains) the Schmidt number is unity.

The decoupling from the turbulence is described by a Schmidt number that is larger than unity. Various expressions for the Schmidt number have appeared in the literature. We adopt:

$$\mathrm{Sc} = (1 + \mathrm{St}), \tag{13}$$

where St is the Stokes number. The Stokes number St is defined as the ratio of the friction time $t_{\rm fric}$ and the eddy turnover time $t_{\rm edd}$. The latter depends not only on the turbulence parameter α, but also on the typical velocity of the largest eddies. This eddy velocity may depend on the type of turbulence (e.g. shear turbulence, convective turbulence, magneto-rotational turbulence), and it is not clearly agreed in the literature what it should be. Therefore we parameterize it in the following way:

$$v_{\rm edd} = \alpha^q c_{\rm s}, \tag{14}$$

where $v_{\rm edd}$ is the average velocity of the largest eddies and q a "'turbulence parameter" between 0 and 1. Schräpler & Henning take $q = 1/2$ in their calculations. The typical largest eddy size $l_{\rm edd}$ can be found by the definition that $D_0 \equiv l_{\rm edd} v_{\rm edd}$. One obtains $l_{\rm edd} = \alpha^{1-q} H_p$. This leads us to an expression for the eddy turn-over time $t_{\rm edd} \equiv l_{\rm edd}/v_{\rm edd} = \alpha^{1-2q}/\Omega_{\rm K}$. The Stokes number then becomes:

$$\mathrm{St} = \frac{t_{\rm fric}}{t_{\rm edd}} = \frac{3}{4}\frac{m}{\sigma}\frac{\Omega_{\rm K}}{\rho c_{\rm s}}\alpha^{2q-1}. \tag{15}$$

In this paper we will take $q = 1/2$, following Schräpler & Henning.

The turbulent α parameter used here is proportional to the $\alpha_{\rm accr}$ of the accretion process in the disk. Traditionally this is denoted as:

$$\alpha = \mathrm{Pt}\ \alpha_{\rm accr} \tag{16}$$

where Pt is the Prandtl number, which is a dimensionless constant of order unity. In this paper we assume it to be Pt = 1 for the vertical turbulence.

2.3. Equilibrium between stirring and settling

High above the midplane the densities of the gas are so low that turbulence is not able to effectively mix the grains upward. Instead the grains settle to the midplane unhindered with a velocity given by Eq. (8). At some height z above the equator the densities become high enough for the turbulent eddies to start to counteract the settling. This height can be estimated by comparing the time scale for settling $t_{\rm sett}$ to the time scale for diffusion $t_{\rm stir} = z^2/D$ which obeys

$$t_{\rm stir} = \frac{\mathrm{Sc}}{\alpha\Omega_K}\frac{z^2}{H_p^2}. \tag{17}$$

By equating $t_{\rm stir} = \xi t_{\rm sett}$ (where ξ is a factor described below) one obtains the following equation in z:

$$\frac{H_p^2}{z^2}\exp\left(-\frac{z^2}{2H_p^2}\right) = \frac{3\sqrt{2\pi}}{4}\frac{m}{\sigma}\frac{\mathrm{Sc}(z)}{\xi\alpha\Sigma}. \tag{18}$$

By taking $\xi = 1$ and solving for z (taking into account that Sc is a function of z), one obtains the height $z_{\rm sett}/R$ down to which the grains of a typical size and mass tend to settle. Below this height the turbulent diffusion manages to sweep up the grains and keep them afloat. The abundance for grains of this size is almost constant below this height. Above this height the abundance decreases because dust can settle down to lower altitude. It should be noted, however, that the transition from fully mixed to fully depleted is not extremely sharp. As will be shown in Sect. 3, by solving Eq. (18) with $\xi = 100$ one obtains a good estimate of the "depletion height" $z_{\rm depl}$ above which the turbulence is so ineffective that dust grains of this size have depleted almost entirely. The transition from well-mixed to dust-free takes place between $z_{\rm sett}$ and $z_{\rm depl}$. For grains smaller than 100 μm the Schmidt number Sc is almost always close to 1 at $z_{\rm depl}$ and below. The decoupling of the grains from the turbulence therefore has only a marginal effect on the solutions.

2.4. Steady state analytic estimates

Based on the above equations one can now make figures of these quantities for a particular disk model. Consider a T Tauri star of mass $M_* = 0.5\ M_\odot$, radius $R_* = 2.5\ R_\odot$ and effective temperature $T_* = 4000$ K. Surround it with a disk with a gas+dust surface density $\Sigma(R)$ given by

$$\Sigma(R) = \Sigma_0\left(\frac{R}{1\ \mathrm{AU}}\right)^p \tag{19}$$

with $p = -1.5$ and $\Sigma_0 = 400$ g/cm^2, with an inner radius of $R_{\rm in} = 0.1$ AU and and out radius $R_{\rm out} = 400$ AU. The disk mass, for this configuration, is $M_{\rm disk} = 0.011\ M_\odot$. We will assume, for the time being, that the disk is vertically isothermal, with a temperature $T(R)$ that is determined by the irradiation of the disk by the central star. We ignore viscous heating, but we discuss its effect in Sect. 5.2. In order to keep things simple and analytic, we *assume* that the flaring angle ϕ (see Chiang & Goldreich 1997 for the definition) is a constant, and has a value of $\phi = 0.05$, which is not too far from realistic values. By equating the irradiation flux $F_{\rm irr} = \phi L_*/(4\pi R^2)$ to the cooling flux $F_{\rm cool} = \sigma_s T(R)^4$ one can solve directly for $T(R)$, obtaining:

$$T(R) = \phi^{1/4}\sqrt{\frac{R_*}{R}}\,T_*. \tag{20}$$

We ignored geometric effects of order z/R. Given the temperature $T(R)$, the vertical density structure is then given by Eqs. (3), (5), (6). Note that this disk structure is highly simplified, and in particular the assumption that ϕ is a positive constant is often untrue. But for the purpose of this paper it is sufficient. Throughout this paper the dust specific weight is taken to be 3.6 g/cm^3 and the mean molecular mass is taken $\mu = 2.3$.

In Fig. 1 the resulting $z_{\rm depl}/R$ and the time scale at which the equilibrium state is reached are shown for the case of $\alpha = 0.01$ and $q = 1/2$. In Fig. 2 the same is shown, but this time for $\alpha = 0.0001$. Shown in the left panels in both figures is a grey line, which indicates the initial height of the $\tau = 1$ surface for radially outward moving stellar photons before the grains have started to settle. It is interesting to observe that for the $\alpha = 0.0001$ case the height $z_{\rm depl}/R$ below which the grain settle (even the 0.1 μm grains) is below this initial $\tau = 1$ surface height. Since dust grains carry virtually all of the opacity of the

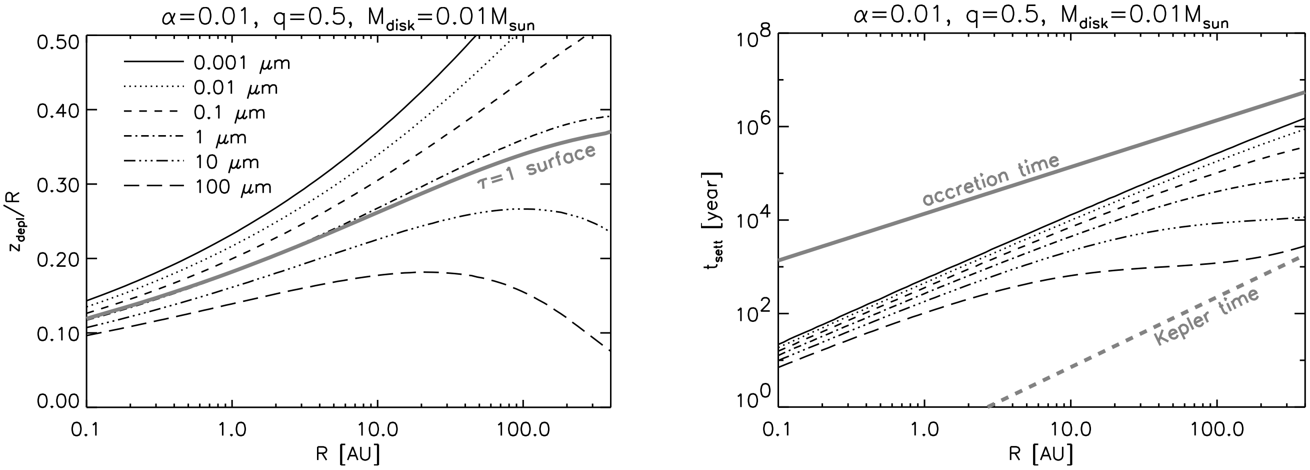

Fig. 1. *Left*: the dust depletion height $z_{\rm depl}$ for the disk model described in the text, for $\alpha = 0.01$ and $q = 1/2$. This is the height above which virtually all grains of a certain size have been removed by settling, once the equilibrium settling-stirring solution is reached. The solid grey curve shows the $\tau = 1$ surface of the disk at $\lambda = 0.55$ μm if the dust has not yet settled and the opacity is dominated by grains smaller than 0.1 μm. *Right*: the time scale $t_{\rm sett}$ for reaching such an equilibrium. This is computed from Eq. (10) with $z = z_{\rm sett}$ (i.e. not with $z = z_{\rm depl}$, since we are interested here in finding the time scale for the entire vertical equilibrium to set in). The solid grey curve is the viscous (i.e. accretion) time scale $t_{\rm accr} = R^2/\nu$. The dotted grey curve is the Kepler time scale $t_{\rm Kep} = 1/\Omega_K$. Since the settling cannot happen on a time scale smaller than this $t_{\rm Kep}$, we have added $t_{\rm Kep}$ to the plotted time scale to ensure this minimum. The annotation for the black curves is the same as in the left panel.

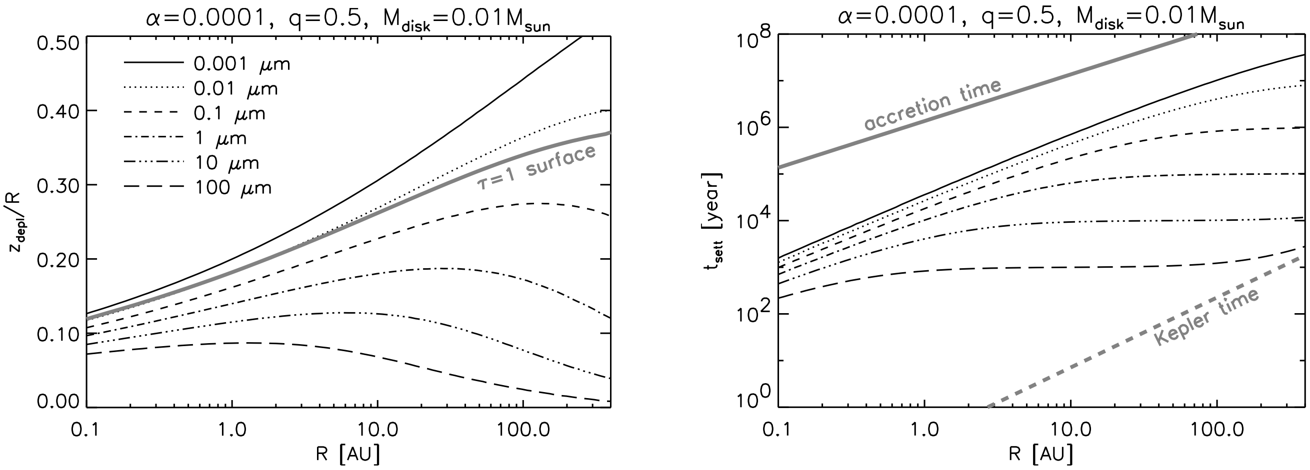

Fig. 2. As Fig. 1, but now for $\alpha = 0.0001$.

disk, this means that when the grains settle, the photospheric surface height $H_{\rm s}$ of the disk is reduced, i.e. the optical appearance of the disk becomes flatter. Also the infrared emission from the disk is reduced as the disk then captures less stellar flux.

The steady state is always reached on a shorter time scale than the accretion time scale ($t_{\rm accr} \equiv R^2/\nu$). It is shorter at small radii than at larger radii, but beyond a certain radius it stays constant. This is because these grains have settled below one pressure scale height, and for $\Sigma \propto R^{-1.5}$ the time scale for a grain to settle down to one pressure scale height or lower is independent of radius (25). The settling time scale for 0.1 μm grains at a few hundred AU ($\sim 10^6$ year) is not much smaller than the typical life time of protoplanetary disks ($\sim 10^6 \cdots 10^7$ year).

An important feature of the steady state solutions is that the $z_{\rm depl}(R)/R$ does not always form a flaring shape. Beyond a certain radius $R_{\rm turn}(a)$ (different for different grain sizes), the value of $d(z_{\rm depl}(R)/R)/dR$ becomes negative. If the disk has only one grain size, and assuming that $z_{\rm depl}$ is a good estimate of the resulting surface height $H_{\rm s}$ of the disk, this would imply that the disk has an $H_{\rm s}/R$ that is not a monotonically increasing function of R. This is a strong indication that *self-shadowing effects* play a role in such disks: the outer disk has a lower $H_{\rm s}/R$ than the intermediate regions and therefore resides in the shadow of these intermediate disk regions (note that if one defines $H_{\rm s}$ to be the location of the $\tau = 1$ surface for radially-outward moving photons, a lower $H_{\rm s}/R$ at larger radii is meaningless because of the shadowing; see Fig. 6). For the case of $\alpha = 0.01$ and 0.1 μm grains this effect is small. One must go to 10 or 100 μm grains to see this effect. For $\alpha = 0.0001$ this effect already takes place with 0.1 μm grains.

In the calculations shown above the Stokes number remains mostly well below unity for grain sizes up to 100 micron. However, if we take $q = 0$, the Stokes number becomes significantly larger than unity beyond the point where

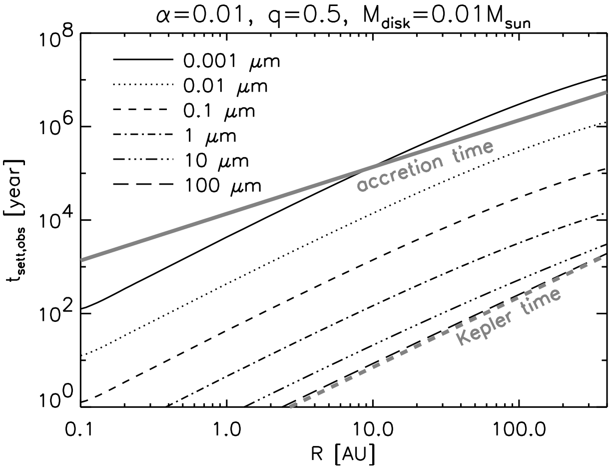

Fig. 3. The time scale with which grains settle below the $\tau = 1$ surface. The solid grey curve is the viscous (accretion) time scale for $\alpha = 0.01$. The dotted grey curve is the Kepler time scale $t_{\rm Kep} = 1/\Omega_K$. Since the settling cannot happen on a time scale smaller than this $t_{\rm Kep}$, we have added $t_{\rm Kep}$ to the plotted time scale to ensure this minimum.

$d(z_{\rm depl}(R)/R)/dR$ becomes negative. This increases the shadowing effect since the $z_{\rm depl}(R)$ drops more quickly as a function of R than for the case $q = 1/2$. The radius $R_{\rm turn}$ of this turn-over point, however, does not change considerably.

It should be noted that the time scale for the settling can be deceptive. It is the time scale it takes to reach the stationary state: the equilibrium between turbulence and settling. But the very upper parts of the disk get depleted from dust more quickly, since the dust settling velocity increases with the decreasing density. The time scale for settling of 0.1 μm grains in the very outer regions of the disk is therefore an upper limit of the settling time: on a much shorter time the dust may settle down below the $\tau = 1$ surface of the disk, which means that settling can quickly affect the shape of the photospheric surface of the disk. In Fig. 3 the time scale is shown within which grains settle below the $\tau = 1$ surface. This $\tau = 1$ surface is computed for radially outward moving photons, using only the absorption opacity for silicate grains of 0.1 μm size at $\lambda = 0.55$ μm (i.e. $\kappa = 2 \times 10^3$ cm^2/g), and is shown as the grey curve in Figs. 1 and 2.

3. 1-D vertical models: How the upper layers deplete

The analytic estimates presented above give a feeling for the spatial and time scales on which the dust settling takes place. If we would only be interested in the steady state solution, we could also use the analytical expressions derived by Dubrulle et al. (1995). However, in order to see how an initially fully mixed disk evolves through settling, we prefer to use a numerical solution from which we can extract the time variations. We do this in two steps. First we take a close look at the local solution at a given distance from the star. In Sect. 4 we will then integrate over the entire disk in order to study the emerging SED and disk images.

Using the expressions for the settling velocity and the turbulent diffusion coefficient presented in Sect. 2, it is straightforward to derive a one-dimensional vertical advection-diffusion equation for the motion of grains. In this one-dimensional approximation we neglect radial migration of the grains due to gas drag or other effects (Weidenschilling 1977). Also we ignore the accretional evolution of the disk itself, or radial mixing phenomena. We only consider the vertical motions of the grains induced by settling and vertical turbulent stirring. We write the distribution function of grains of mass m located at height z above the midplane as $f(m,z)$. It is defined such that $f(m,z)\,dm\,dz$ represents the number of grains (of this size, at this height) per square cm of disk.

For the gas we use again a Gaussian density profile and isothermal temperature profile. We assume that during the dust settling process this gas density and temperature profile do not change with time.

The conservation equation for the dust grains is (ignoring the R coordinate for compactness):

$$\frac{\partial f(m,z)}{\partial t} - \frac{\partial}{\partial z}\left[\rho_{\rm gas} D(m,z)\frac{\partial}{\partial z}\left(\frac{f(m,z)}{\rho_{\rm gas}}\right)\right] + \frac{\partial}{\partial z}\left(f(m,z) v_{\rm sett}(m,z)\right) = 0. \tag{21}$$

This equation is valid if no dust coagulation takes place.

We take the same stellar parameters as in Sect. 2, and the same disk setup. We take our slice at $R = 10$ AU, which means that the gas surface density at that point is $\Sigma = 13$ g/cm^2. We simulate the settling of 0.1 μm grains and adopt $\alpha = 0.0001$ for the turbulence. In Fig. 4 the evolution of the dust settling is shown for this slice, and a comparison of the stationary solution (which is reached at about $t = 3 \times 10^5$ yr) to the analytic estimates is given as well.

One can see that as the grains settle, the upper parts of the disk are entirely depleted from dust. After only 10^3 years the depletion above $z/R = 0.30$ is a factor of 10^{-10} and above $z/R = 0.325$ it is 10^{-30}. This means that long before a steady state is reached, the regions above $z/R = 0.30$ are already completely dust-free. One can see in Fig. 4-left that the dust that has settled forms a layer on top of the disk in which the dust-to-gas ratio is slightly above 0.01. This is simply the piling-up of the settled dust from higher region of the disk.

It is interesting also to see that while the dust is still settling it has a very sharply defined surface. Below a certain z the dust-to-gas ratio is about 0.01, and just a small step above this z the dust-to-gas ratio is almost zero. This sharp transition is a consequence of the fact that initially all grains are settling with the equilibrium settling velocity, unperturbed by stirring. Since the settling speed decreases towards the mid-plane, the uppermost grains catch up with grains just below them and therefore produce a very sharp boundary. In the later stages, when the steady state has been reached, this sharp cut-off softens, but it should still be noticed that beyond $z \simeq 0.23R$ the depletion increases very fast.

The $\tau = 1$ surface of the disk, i.e. the disk's photosphere, for silicate grains of 0.1 μm at $t = 0$ (i.e. the well-mixed case without settling) lies in this example at about $H_s/R = 0.3$. Note that this is the $\tau = 1$ surface for the stellar radiation which enters the disk under a grazing angle of $\phi = 0.05$. After 10^3 years

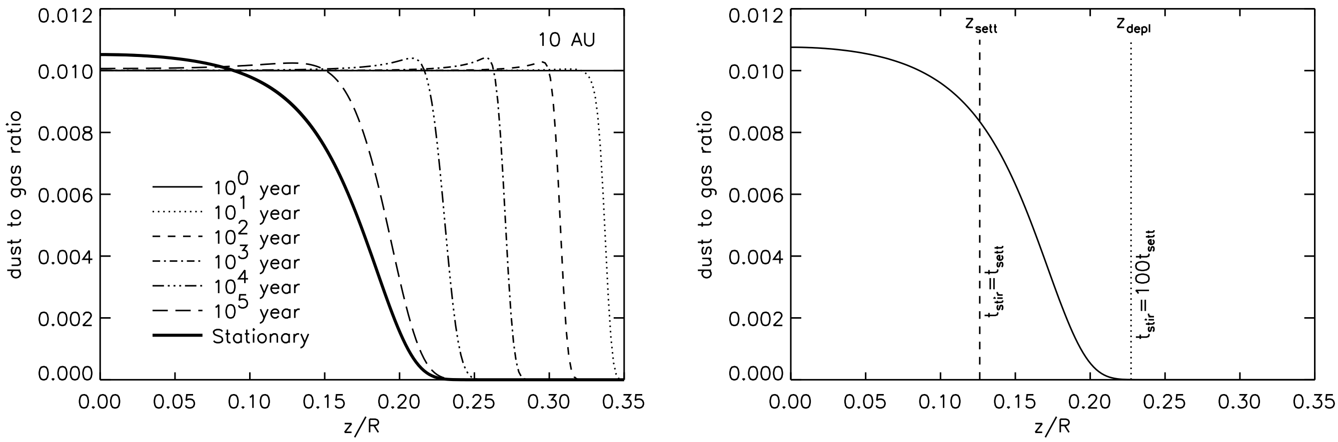

Fig. 4. The dust-to-gas ratio in a 1-D vertical slice at 10 AU in the standard disk model with $\alpha = 0.0001$, assuming 0.1 μm size grains. At the start ($t = 0$) the dust is well-mixed with the gas, i.e. the dust-to-gas ratio is constant (we take it 0.01). *Left*: the time sequence. *Right*: the stationary solution compared to the analytic estimates. The vertical lines are the computed values of $z_{\rm sett}$ and $z_{\rm depl}$ (from left to right). These are defined to be solutions of Eq. (18) with $\xi = 1$ and $\xi = 100$ respectively. As one can see, $z_{\rm depl}$ is a good definition of the height above which the depletion is almost perfect.

the dust has settled well below this point, meaning that the dust will take its $\tau = 1$ surface along with it toward lower z (as already predicted in Sect. 2). In other words: after 10^3 years the photospheric surface height of the disk $H_{\rm s}$ is reduced as a result of dust settling. The gas still remains at higher z, but it is the dust that carries the opacity and determines the disk's appearance.

4. 1+1-D disk models: SEDs and images

As we have seen above, dust settling can strongly affect the shape of the $\tau = 1$ surface $H_{\rm s}(R)$ of the disk. This shape determines for a large part the thermal infrared emission from this disk and also the appearance of images in scattered light. If the disk's surface has a strongly flaring shape, one expects a spectral energy distribution (SED) with a strong emission, particularly at mid- and far-IR wavelengths. If the disk has such a shape that the outer regions are shadowed by the inner regions (if $H_{\rm s}/R$ decreases with radius), then the expected SED has a rather weak far-IR excess. The predicted images in scattered light for these two cases are also expected to be very different. It is therefore of crucial importance to investigate how the shape of the disk changes as a result of dust settling.

We again start with the simple model described earlier, and we do a 1-D dust settling calculation at every radius, taking a radial grid of 20 grid points in R. In this way we simulate the entire disk in a 1+1-D manner. We take $\alpha = 0.00001$, i.e. a factor of ten smaller than taken in Sect. 2.4, in order to accentuate the effects of settling on the appearance of the disk. At $t = 1$, $10, \ldots, 10^6$ years we apply a 2-D radiative transfer code (called RADMC[1]) to the given dust distribution, and compute the SED of the disk at these times. Also we compute the intensity of scattered light as a function of distance from the star, i.e. the brightness of an images of the disk in scattered light at $\lambda = 1.65$ μm.

[1] www.mpa-garching.mpg.de/PUBLICATIONS/DATA/radtrans/radmc/

The dust temperature computed by RADMC is likely to differ somewhat from the dust/gas temperature $T(R)$ assumed as input to the density structure of the disk. In principle one should iterate the computation of the temperature and the density structure to obtain a self-consistent model as we did in DD04. However, since our main interest is the process of dust settling rather than the details of disk structure, we ignore this feedback for the sake of simplicity.

4.1. Model with single grain size

The first model (model A) only has grains of 0.1 μm size. In Fig. 5-left the SED as a function of time is shown. The SED changes only barely on time scales smaller than 10^5 years. But on time scales longer than 10^5 years the far-IR flux drops. Two effects play a role in reducing the far-IR flux. First of all, due to the settling, the surface height of the disk $H_{\rm s}$ has been reduced. Since the thickness of a disk is directly related to the total amount of stellar radiation captured and reprocessed by the disk, this effect reduces the integrated IR emission over the entire wavelength domain. Chiang et al. (2001) used this fact to argue that dust settling may be responsible for the low far-IR flux of some Herbig Ae/Be star. The other, more important reason for the reduction of the far-IR flux is that due to the turn-over in the $H_{\rm s}/R$ beyond $R = R_{\rm turn}$, the outer disk is *shadowed* by the inner regions of the disk. This means that these outer regions are irradiated only in an indirect way, for example by light that scattered off dust grains hovering slightly above the photosphere at the turn-over (i.e. self-shadowing) radius $R_{\rm turn}$, or by radial radiative diffusion (see DD04 for a discussion of self-shadowed disks).

The time evolution of the scattering intensity shows a very interesting behavior, as is shown in Fig. 5-right. Initially, the scattering intensity changes only in the innermost regions (inward of 10 AU), from the inside out. After about 10^5 years, the inner disk stabilizes – the steady state solution is reached there. By this time the outer part of the disk up to 100 AU

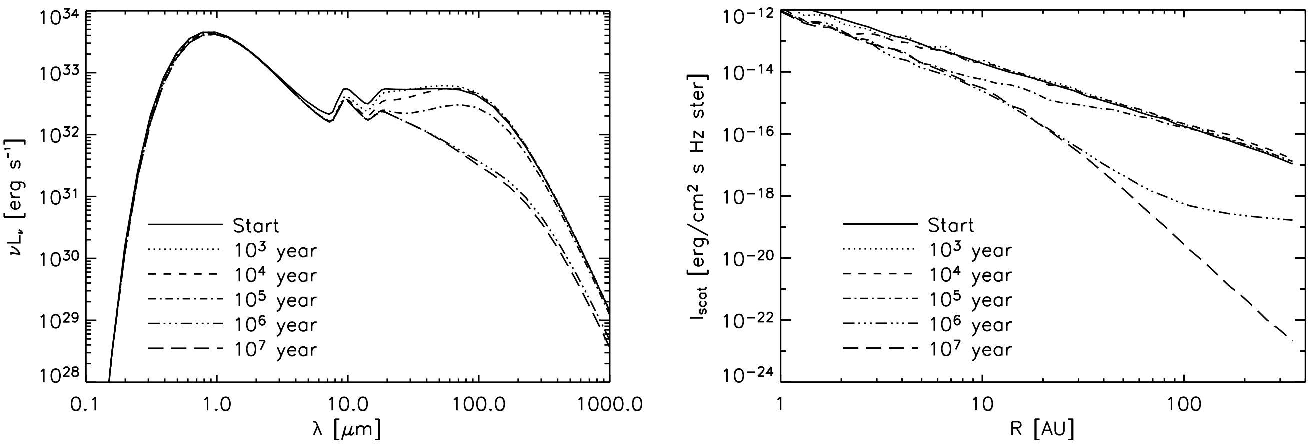

Fig. 5. The SED (*left*) and the 0.55 μm scattering intensity (*right*) of the disk as a function of time for the 1+1D model with a single grain size of $a = 0.1$ μm. Note that the time intervals are logarithmic (a factor of 10 apart). The disk is seen face-on.

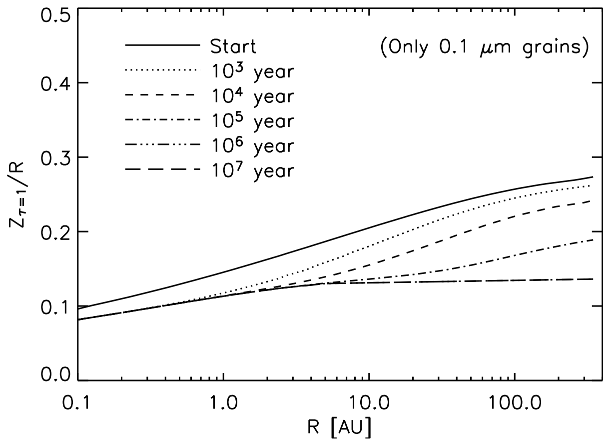

Fig. 6. The shape of the $\tau = 1$ surface, where the optical depth τ is at 0.55 μm and is measured *radially* from the stellar surface outward (i.e. horizontally in the figure). For this reason the $\tau = 1$ surface is a monotonically increasing function of R, even when the disk fully collapses beyond some point. This is indeed apparent in this figure, because it appears if beyond 10^6 and 10^7 years nothing changes, whereas the scattering image still becomes dimmer in this time frame (Fig. 5).

starts to be affected by the settling. After 10^6 years, the scattering intensity is already reduced by more than a factor of 100, and after 10^7 years in the outermost regions, the reduction is even 10^6. This is clear evidence of the self-shadowing effect operating in these regions. Without shadowing, a much more gradual change like the one seen in the inner regions would occur also here. A self-consistent computation of the disk structure would only enhance this effect since the temperature in the outer disk will drop and lead to a reduced disk scale height. In Fig. 6 the self-shadowing effect is shown by the shape of the $\tau = 1$ surface for radially outward moving stellar photons. Up to 10^5 years the z/R location of the $\tau = 1$ surface still increases for increasing R, which is indicative of a flaring geometry. But after 10^6 years the $\tau = 1$ surface stays essentially at constant z/R beyond about 7 AU, which indicates that the disk is shadowed beyond 7 AU.

4.2. Model with grain size distribution

In Sect. 2 we have shown that the settling behavior of grains varies strongly with grain size. It may be possible to represent the grain size distribution with a typical size for a specific application, but the correct size to use will depend upon the application. The intensities seen in scattered light is dominated by one grain size, the infrared emission by another grains size, and other indicators like PAH emission will depend on yet another grain type. Therefore we now show the results of a calculation in which we include a full size distribution. The grains of each size settle with their own settling velocity and have their own Schmidt number. The bigger grains will settle much faster and deeper than the smaller ones, so that one obtains a different grain size distribution at different heights above the midplane. As our initial grain size distribution we take an MRN distribution (Mathis et al. 1977) between grain sizes of 0.005 μm and 0.25 μm. The original MRN distribution is only well constrained down to grain sizes of about 0.02 μm (18). However, in order to see what the influence of smaller grains would be we extend the size distribution down to 0.005 μm.

The results are shown in Fig. 7. The same shadowing effects are seen as in the case of the single 0.1 μm size grains, although there are also some differences. It is interesting that this shadowing in fact takes place also for the MRN distribution, even though the very smallest grains clearly stay afloat much higher up. However, these small grains have relatively low opacity at the stellar wavelengths: the opacity is highest for grains between 0.1 μm and 1 μm. Moreover the MRN distribution goes as $m^2 f(m) \propto m^{1/6} \propto a^{1/2}$, meaning that most of the mass is concentrated in the bigger grains. So even if the opacity of the grains (per gram dust) would be independent of grain size (up to 1 μm), still the opacity will be dominated by the $0.1 \cdots 1$ μm grains. Therefore the very small grains will not account for much of the reprocessing of stellar radiation into the infrared. Since the albedo of the small grains at stellar wavelengths is virtually zero, they will not contribute at all to the scattering of starlight into the line of sight. In effect, only the grains larger than roughly 0.03 μm will contribute significantly to the reprocessing and scattering. Therefore, even

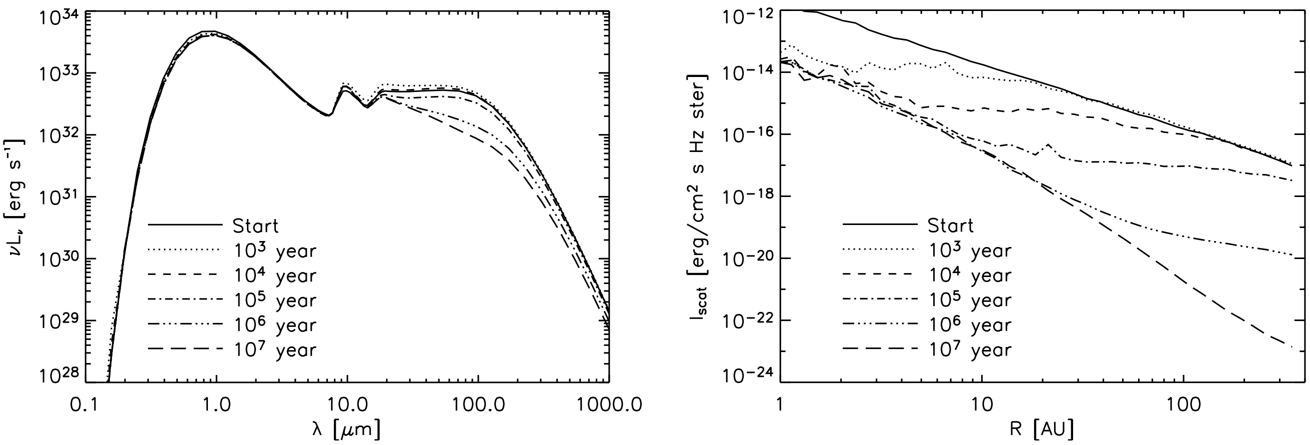

Fig. 7. As Fig. 5, but for the disk model with an MRN grain size distribution.

though the very small grains virtually do not settle at all, the *relevant* grains ($a \gtrsim 0.03\ \mu$m) *do* settle.

This has two effects, both of which contribute to the dimming of the scattering image. First, the large grains which are most reflective fall below the $\tau = 1$ surface of the small grains (which are not reflective). The small grains may therefore partly shield the larger (reflective) grains from stellar light, thereby dimming the scattering image. This "differentiation" effect is clearly seen in Fig. 7 as an overall dimming of the disk even in regions which are clearly non-shadowed. This dimming is quite strong in this case, but for higher values of α this effect is reduced. As expected, such an overall dimming is absent in the single-grain-size case (Fig. 5). Secondly, the $\tau = 1$ surface itself is dragged down by settling, creating a self-shadowed geometry similar to the one for the single grain size simulation. The fact that even in this MRN simulation the disk becomes partly self-shadowed can be seen from Fig. 8, where the evolution of the $\tau = 1$ surface is shown for the MRN model. But it can also be seen from this figure that the shadowing is not as sharp as in the case of a single 0.1 μm grain. Indeed, the weakening of the far-infrared flux for the MRN case is less pronounced than in the single-grain model. For the scattered light intensity the effect of self-shadowing is still clearly seen, though the dimming by the "differentiation" effect may, for these low values of α, be equally important for the (non-)detection of disks in scattered light.

In Fig. 7-left the evolution of the SED is shown for the MRN model. Interestingly, the mid- to far-infrared excess first slightly brightens (between 0 and 10^4 years). Only afterwards the mid- to far-infrared excess starts to decline, eventually becoming rather weak at $10^6 \cdots 10^7$ years. This initial brightening is because due to the quick settling in the inner region, while the outer regions take a longer time, the flaring angle of the surface of the disk temporarily increases. Only after the outer regions start to sink into the shadow of the intermediate disk regions the mid- to far-infrared excess starts to decrease significantly.

Figure 9 shows images of the disk at 0.55 μm at inclination 45°. We truncated the disk to 100 AU so that both the inner regions and the outer regions can be seen clearly.

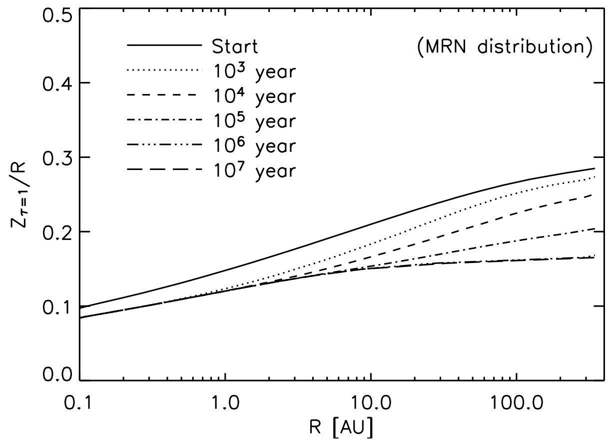

Fig. 8. As Fig. 6, but for the MRN model.

5. Discussion

5.1. Scaling of the results

The analytic formulae of Sect. 2 and the numerical models of Sect. 3 can easily be scaled to the case of fluffy grains. The critical parameter that goes into all these equations is the ratio of grain geometric cross section and grain mass: σ/m. A compact silicate grain with a specific weight of $\chi = 3.6$ g/cm^3 and a size of $a = 0.1\ \mu$m has $\sigma/m = 3/(4a\chi) = 2 \times 10^4$ cm^2/g. A fluffy grain of size 10 μm but the same value of $\sigma/m = 2 \times 10^4$ cm^2/g will behave exactly the same as the compact 0.1 μm size grain.

5.2. The role of viscous dissipation

Throughout the paper we have taken a very simple temperature and density structure of our disk. In reality the structure of an irradiated disk will be more complex (see e.g., Dullemond et al. 2002; DD04). Moreover, if the viscous heating by active accretion is included, the midplane can become considerably hotter than in our simple model. While a detailed inclusion of these effects is beyond the scope of this paper, it is instructive to make some estimates.

The midplane temperature for a disk heated only by viscous dissipation is given by $T^3_{\rm v,mid} = (27/64)(\alpha\kappa_R k/\sigma\mu m_p)\Sigma^2\Omega_K$,

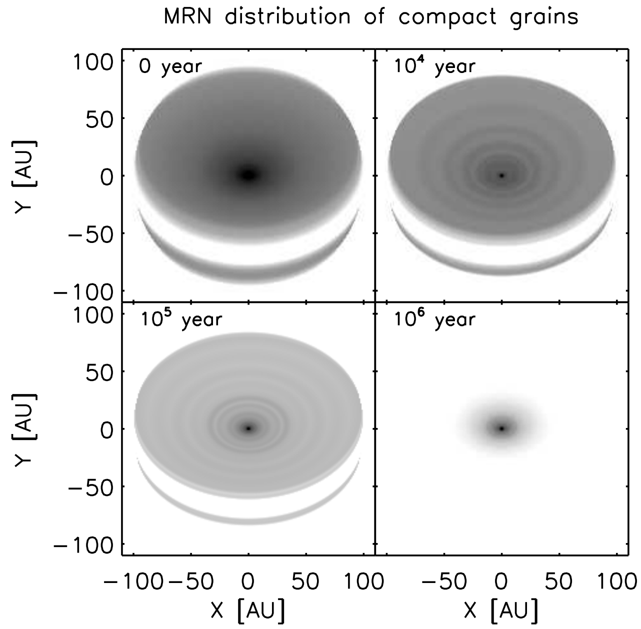

Fig. 9. Images of the $\alpha = 0.00001$ disk model with an MRN distribution of compact grains (see Fig. 7), seen at an inclination of 45° at $\lambda = 0.55\,\mu$m. For these images the model was truncated at 100 AU, so that both the inner regions ($\simeq$25 AU) and the outer regions ($\approx$100 AU) can be seen clearly. The images are at 0, 10^4, 10^5 and 10^6 years. The gray scale is logarithmic intensity (inverse video). Note that the central star is not included in these images (a perfect coronograph).

and the surface temperature ("effective temperature") is given by $T_{\rm v,eff} = (8/3\kappa_R\Sigma)^{1/4}\,T_{\rm v,mid}$, where κ_R is the Rosseland mean opacity of the dust + gas mixture (before settling). By finding the radius beyond which the $T_{\rm v,mid}$ and $T_{\rm v,eff}$ fall below the temperature given by Eq. (20), we can estimate beyond which radii the viscous heating becomes unimportant at the midplane and the surface respectively. For the model parameters given in Sect. 2.4, for the case of $\alpha = 0.01$ these radii are 5 AU and 0.6 AU, for $\alpha = 0.0001$ they are 1 AU and 0.05 AU, and finally for the case of $\alpha = 0.00001$ these are 0.5 AU and 0.02 AU respectively. At large radii the viscous heating is therefore not important, but it may be important at small radii.

An increase in temperature due to viscous heating will increase the friction of the particles, and it will also increase the pressure scale height of the disk. These combined effects will increase the height of the photosphere after a settling equilibrium has set in. Since viscous heating is unimportant at large radii, and therefore the increase in height of the disk takes place predominantly at small radii, the effect of inclusion of viscous dissipation is likely to increase the shadowing effect.

5.3. Geometries

In our earlier paper (DD04) we have demonstrated, on the basis of theoretical models, that disks around Herbig Ae/Be stars come in two main shapes: flared disks and self-shadowed disks. In the self-shadowed case, the inner rim of the disk casts a shadow over the entire disk behind it. The cause for the self-shadowing was a reduction of opacity due to grain growth.

In the present paper we consider another process: dust settling. We ignore grain growth. Moreover, we focus mainly on T Tauri stars, in which the effect of the puffed-up inner rim is likely to be less pronounced, and we ignored it here. In this setup we find geometries very similar, though not identical to DD04. We start out with a flaring disk, and after settling we may obtain a partly self-shadowed disk, dependent on the value of α. In contrast to the self-shadowed disk solutions of DD04 our self-shadowed solution are only self-shadowed outside of a few AU, while they remain flaring inside of this radius. And the shadow is cast by the flaring inner part of the disk instead of the puffed-up inner rim. In Fig. 10 the two geometries are shown.

For Herbig Ae/Be stars the inner rim cannot be ignored that easily. It may happen that dust settling could cause the entire disk to fall into the shadow of the inner rim, producing the fully-self-shadowed geometry presented in DD04, but in a different way than was shown by DD04. However, dust settling also affects the puffed-up inner rim, and this is more difficult to model in detail. The inner rim is much hotter than the rest of the disk. A higher abundance of free electrons would cause the magneto-rotational instability to operate more efficiently here and increase turbulent stirring. Including the inner rim into the analysis is therefore a subtle matter, which we defer to a future paper.

5.4. SED type versus scattering images

In DD04 we showed that for Herbig Ae stars, disks dominated by small grains usually have flared geometries, while disks in which most of the small grains have coagulated to big grains are usually self-shadowed. The SEDs of these two kinds of disks were very reminiscent of the two types of SEDs found among the SEDs of Herbig Ae/Be stars (the "group I" and "group II" sources of Meeus et al. 2001). It was therefore suggested that group I sources are flared disks and group II sources are self-shadowed disks. This suggestion has passed several observational tests, including the identification of UX Orionis stars with group II sources (Dullemond et al. 2003), the presence or absence of PAH emission features (Acke et al. A&A submitted), and the correlation of the group I/II identification with the (sub-)mm slope of the source (Acke et al. submitted). The self-shadowed solutions in DD04 were caused by a simple optical depth effect: when most of the small grains are turned into a few big ones, the optical depth is greatly reduced. The disk then gradually becomes self-shadowed, since at large radii the optical depth is not sufficient to keep its surface above the shadow of the inner rim. In the current study we now show that also *dust settling* may turn a flared disk into a self-shadowed one. In reality, it is most likely a combination of *settling and coagulation* leads to the observed effects.

It was mentioned in DD04 that self-shadowed disks are expected to have weak scattering images, for the obvious reasons that direct stellar radiation cannot irradiate the disk. But it was also shown that only for extreme parameters the self-shadowed disk solutions that follow from well-mixed models are very deeply shadowed. We estimate that for a fully mixed model,

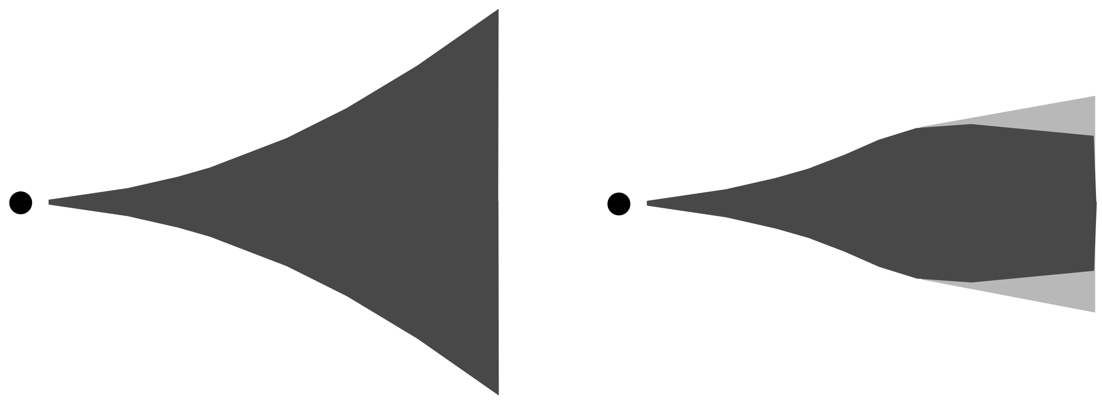

Fig. 10. Pictograms of the two geometries. *Left*: the flaring disk we start out with. *Right*: after settling the outer parts of the disk are self-shadowed. Note that whether this partly self-shadowed geometry is obtained depends whether the turbulence is low enough.

the scattering intensity of the disk is reduced by typically a factor of 10. In the present paper we now show that dust settling can cause a much stronger shadowing effect. It can remove all grains capable of scattering stellar radiation (i.e. grains larger than about 0.03 μm size) from the upper layers of the disk, so that if self-shadowing occurs in this way, the expected scattering images are extremely weak. Therefore, group II sources have weaker scattering images than group I sources. If, on top of that, it is found that the group II sources are *orders of magnitude* weaker, then it is clear that dust settling must also play a role.

5.5. Timescales

The most realistic simulation in our study is the run involving an MRN grain size distribution. As shown in Figs. 7 and 8, the changes in the SED and in the scattering image brightness happen largely on a timescale of 10^6 years. Given the fact that the observed T Tauri stars are typically between 1 and 10 Myrs old, this gives an indication that settling might be happening too fast in our simulation. If indeed the settling has happened already after 10^6 years, one would expect most disks to show steep SEDs and weak scattering images. Looking at the sample of Herbig stars studied by Meeus et al. (23), this seems to be consistent in the way that the group II sources[2] have ages larger than 1 Myr while two of the group I sources with available ages are only about 10^5 years old. However, with AB Aur (about 2 Myrs) and in particular HD 100546 (about 10 Myrs), there are two stars in the flaring disk group I which are significantly older. For T Tauri stars, the situation is less clear as the SEDs of T Tauri stars have not yet been classified in the same way as the Herbig stars so far. There may be observational biases involved here: The stars have been selected on IRAS colors which favors the detection of group I sources. If there is a large number of sources with strongly flaring disks at ages much larger than 10^6 years, it is possible that the dust settling study presented here is incomplete. A possible solution could be larger friction between dust and gas in the upper disk layers, due to electrostatic interactions between charged grains and the ionized plasma. Another intriguing possibility is that even the larger interstellar grains are already porous aggregates (21; 29) – an effect which would increase their surface area and therefore their drag coupling to the gas. And finally, it could be possible that, for some unknown reason, some disks are more turbulent than others. The more turbulent disks then remain flaring while the quiescent disks will become self-shadowed in a very short time. If this is true, then this would imply that group II sources are not evolutionarily linked to group I sources. However, since many indications point toward such an evolutionary link, and since there seems to be no good reason why some disks are more turbulent than others (other properties remaining the same), we consider this scenario less likely.

[2] 51 Oph is a special case of a star with an extremely low IR excess and is therefore not considered here.

6. Conclusion

We find that dust settling can change the shape of the photosphere of protoplanetary disks on time scales of less than 10^3 years at small radii ($\lesssim$10 AU) and 10^5 years at larger radii. On a time scale shorter than 10^6 years a equilibrium state sets in in which settling is balanced by turbulence. In the equilibrium state the photosphere of the disk may have a partly self-shadowed shape, so that the outer regions of the disk are not anymore directly exposed to the stellar radiation. They are only indirectly heated by infrared emission from other parts of the disk.

Close to the star the settling in the upper layers of the disk proceeds much faster than at large radii, and an equilibrium solution is therefore reached more quickly. This means that the reduction in the photospheric height of the disk ($H_s(R)$) first happens at small radii, and then happens at progressively larger radii, until after about 10^5 to 10^6 years the equilibrium state has been reached globally. The transition from flaring disk to half-flaring-half-self-shadowed disk therefore happens on the latter time scale.

The flaring disks (before settling) are expected to have a reasonably strong mid- to far-infrared excess, while the partly self-shadowed disks have a much weaker mid- to far-infrared excess. Moreover, the partly self-shadowed disks should become virtually undetectable in resolved scattered light images beyond the self-shadowing radius, whereas non-self-shadowed disks (early stages) should be much brighter. But even without self-shadowing our calculations show that settling can cause dimming of the disk in scattered light. This is by a "differentiation" process in which the larger/heavier more reflective grains settle deeper into the disk, leaving the smaller/lighter less reflective grains determining the optical appearance of the surface of the disk.

Acknowledgements. C.P.D. wishes to thank C. Grady for stimulating discussions that made us aware of the observational evidence for shadowing in disks. We also thank L. Waters, Th. Henning and J. Cuzzi for very helpful discussions and advice. Finally, we wish to thank the referee, R. Lachaume, for his extensive comments which have improved the manuscript considerably.

References

Augereau, J. C., Lagrange, A. M., Mouillet, D., & Ménard, F. 2001, A&A, 365, 78
Bouwman, J., Meeus, G., de Koter, A., et al. 2001, A&A, 375, 950
Calvet, N., Patino, A., Magris, G. C., & D'Alessio, P. 1991, ApJ, 380, 617
Chiang, E. I., & Goldreich, P. 1997, ApJ, 490, 368
Chiang, E. I., Joung, M. K., Creech-Eakman, M. J., et al. 2001, ApJ, 547, 1077
Cuzzi, J. N., Dobrovolskis, A. R., & Champney, J. M. 1993, Icarus, 106, 102
Cuzzi, J. N., Davis, S. S., & Dobrovolskis, A. R. 2003, Icarus, 166, 385
D'Alessio, P., Calvet, N., & Hartmann, L. 2001, ApJ, 553, 321
Dubrulle, B., Morfill, G., & Sterzik, M. 1995, Icarus, 114, 237
Dullemond, C. P. 2002, A&A, 395, 853
Dullemond, C. P., & Dominik, C. 2004, A&A, 417, 159
Dullemond, C. P., Dominik, C., & Natta, A. 2001, ApJ, 560, 957
Dullemond, C. P., van Zadelhoff, G. J., & Natta, A. 2002, A&A, 389, 464
Dullemond, C. P., van den Ancker, M. E., Acke, B., & van Boekel, R. 2003, ApJ, 594, L47
Eisner, J. A., Lane, B. F., Akeson, R. L., Hillenbrand, L. A., & Sargent, A. I. 2003, ApJ, 588, 360
Grady, C. A., Woodgate, B., Bruhweiler, F. C., et al. 1999, ApJ, 523, L151
Honda, M., Kataza, H., Okamoto, Y. K., et al. 2003, ApJ, 585, L59
Kenyon, S. J., & Hartmann, L. 1987, ApJ, 323, 714
Kim, S., Martin, P. G., & Hendry, P. 1993, BAAS, 25, 806
Leinert, Ch., van Boekel, R., Waters, L. B. F. M., et al. 2004, A&A, accepted
Mannings, V., & Sargent, A. I. 1997, ApJ, 490, 792
Mathis, J. S., Rumpl, W., & Nordsieck, K. H. 1977, ApJ, 217, 425
Mathis, J. S., & Whiffen, G. 1989, ApJ, 341, 808
Meeus, G., Sterzik, M., Bouwman, J., & Natta, A. 2003, A&A, 409, L25
Meeus, G., Waters, L. B. F. M., Bouwman, J., et al. 2001, A&A, 365, 476
Millan-Gabet, R., Schloerb, F. P., & Traub, W. A. 2001, ApJ, 546, 358
Miyake, K., & Nakagawa, Y. 1995, ApJ, 441, 361
Natta, A., Prusti, T., Neri, R., Wooden, D., & Grinin, V. P. 2001, A&A, 371, 186
Przygodda, F., van Boekel, R., Àbrahàm, P., et al. 2003, A&A, 412, L43
Safronov, V. S. 1969, Evolution of the Protoplanetary Cloud and Formation of the Earth and Planets (Moskow: Nauka Press (in Russian)), English translation: NASA TTF-677, 1972
Stepnik, B., Jones, A. P., Abergel, A., et al. 2002, EAS Publications Ser., Proc. of Infrared and Submillimeter Space Astronomy, held 11–13 June, 2001, ed. M. Giard, J. P. Bernanrd, A. Klotz, & I. Ristorcelli (EDP Sciences), 4, 31
Takeuchi, T., & Lin, D. N. C. 2002, ApJ, 581, 1344
Takeuchi, T., & Lin, D. N. C. 2003, ApJ, 593, 524
van Boekel, R., Waters, L. B. F. M., Dominik, C., et al. 2003, A&A, 400, L21
Voelk, H. J., Morfill, G. E., Roeser, S., & Jones, F. C. 1980, A&A, 85, 316
Weidenschilling, S. J. 1977, MNRAS, 180, 57
Weidenschilling, S. J. 1997, Icarus, 127, 290